Title

Analysis of laboratory data on ultrasonic monitoring of permeability reduction due to biopolymer formation in unconsolidated granular media

Journal

Geophysical Prospecting, 64(2)

ISSN

0016-8025

Authors

Berryman, JG
Kwon, T-H
Dou, S
et al.

Publication Date

2016-03-01

DOI

10.1111/1365-2478.12295

Peer reviewed

Analysis of laboratory data on ultrasonic monitoring of permeability reduction due to biopolymer formation in unconsolidated granular media

J.G. Berryman

T.-H. Kwon

S. Dou

J.B. Ajo-Franklin

S.S. Hubbard

First published: 18 August 2015
https://doi.org/10.1111/1365-2478.12295

ABSTRACT

We show how to estimate the fluid permeability changes due to accumulated biopolymer within the pore space of a granular material using laboratory measurements of overall permeability, together with various well-known quantitative measures (e.g., porosity, specific surface area, and formation factor) of the granular medium microstructure. The main focus of the paper is on mutual validation of existing theory and a synthesis of new experimental results. We find that the theory and data are in good agreement within normal experimental uncertainties. We also establish quantitative empirical relationships between seismic and/or acoustic attenuation and overall permeability for these same systems.

INTRODUCTION

Previous studies have shown that ultrasonic P-wave measurements are sensitive to the products of microbial activities in porous media, including biomineralization (Williams *et al*. 2005) and biofilm formation (Davis *et al*. 2009, 2010). In recent work, Kwon and Ajo-Franklin (2011, 2013) performed laboratory column experiments involving stimulated deposition of a biopolymer (dextran) in unconsolidated sediments. A pure culture of the bacteria *Leuconostoc*

mesenteroides was grown in a sucrose-rich environment, whereupon *L. mesenteroides* produced large quantities of dextran. This process, well-documented in the microbiology literature (Lappan and Foggler 1996), is one possible approach for subsurface profile control, which is a method of improving waterflood efficiency for enhanced oil recovery. In the experiments described by Kwon and Ajo-Franklin (2013), column permeability was significantly reduced due to induced pore-clogging effects. A clear P-wave attenuation signature accompanying the pore clogging was observed and monitored. Work presented here provides an analysis of these results and establishes some useful quantitative correlations between these permeability reductions and the accompanying increases in observed ultrasonic wave attenuation.

Related frequency-dependent bender element (BE) measurements of Ta, Kwon, and Muhunthan (2014) show a similar increase in acoustic attenuation along with an observed decrease in bulk permeability as a result of the same pore-clogging effects of the bacterial dextran being injected. These results will also be elaborated in the following discussion.

One important distinction needs to be made before proceeding with the main analysis. All the main analyses presented here are pertinent only to the fast Biot wave, which itself interacts poroelastically with the contents of the pores, and are therefore significantly and measurably attenuated because of these interactions as we show here. Part of the energy loss for the Biot fast wave is due to the viscous damping effects of any fluids in the pore space. Other losses may be thought of correctly as being viscoelastic in nature.

There has been earlier experimental work on granular systems showing that Biot's compressional wave of the second kind (sometimes also called the “slow compressional wave”) can be observed in loosely consolidated granular materials (Nakagawa, Soga, and Mitchell 1997). These experiments were conducted approximately in the frequency range of 2.0–7.0 kHz. This work, however, is not pertinent to the present effort because our focus is on well-consolidated granular media with biopolymers being produced in order to plug the pores and thereby retain fluids being sequestered as long as possible. This target application precludes the possibility of having any significant presence of Biot slow waves in the systems of most interest to us.

PERMEABILITY REDUCTION RESULTING FROM ACCUMULATION OF BACTERIAL BIOPOLYMER

If we accept the following Kozeny–Carman-style model (Berryman 1995) of fluid permeability:

$$\kappa = \frac{\phi^2}{2s^2 F}, \quad (1)$$

where κ is fluid permeability, ϕ is porosity, *F* is the dimensionless electrical formation factor, and *s* is the specific surface area, then we can make some progress towards understanding the significance of permeability data from the laboratory experiments in Kwon and Ajo-Franklin (2011). This formula arises in various circumstances but has been found to be quite accurate (Blair, Berge, and Berryman 1996, 1997) for applications to image processing methods, specifically when care is taken to account properly for certain quantitative issues arising due to errors inherent in the image digitization process (Martys and Garboczi 1992). In similar contexts, some authors (Johnson, Koplik, and Schwartz 1986; Johnson, Koplik, and Dashen 1987; Johnson 1989) replace the ratio $\phi/2s$ by the inverse of the Λ parameter (Johnson *et al*. 1986; Johnson 1989), where Λ is defined here in Appendix APPENDIX A [see Martys and Garboczi (1992)]. Earlier work of Plona (1980) also establishes the presence of secondary bulk compressional waves (now usually called the “Biot slowwaves”) in porous water-saturated glass samples. Berryman (1980) showed that these secondary waves could be quantitatively explained by Biot's theory when supplemented by effective medium theory using needle-shaped tubes to represent and approximate the behaviour of the pore space in the glass samples. Cortis and Berryman (2010) have subsequently shown that, for flow in pores (and therefore related to slow waves in Biot theory) with fractal rough surfaces, the modelling can proceed but needs some special care in certain limiting cases.

Laboratory experimental results of Kwon and Ajo-Franklin (2011, 2013) have shown that the initial sand pack being studied had a permeability of about 5.3 D, where D is one darcy (which is $\mathrm{D} = 1\mu\mathrm{m}^2 = 10^{-12}\mathrm{m}^2$). The Ottawa F110 sand used had a mean particle diameter of about 120 μm, so average grain radius was about 60 μm. The gravimetrically inferred porosity for the column was $\phi \simeq 0.38$. Measured permeability at the end of the experiment was 230 mD versus the initial value of 5.3 D. The resulting overall reduction in permeability was therefore approximately a factor of 23. This reduction was presumably entirely due to the biopolymer-induced pore-clogging effects.

As a first step, we apply the well-known Kozeny–Carman formula (Berryman 1995) shown in equation 1 to obtain a quantitative measure of the grainpack internal pore geometry. This computation is accomplished by using the Kozeny–Carman formula to deduce an effective formation factor *F* from the data available at the beginning of the experiment. The number density of the grains $n = N/V$ (where *N* is the total number of grains in volume *V*) can easily be determined from the relationship:

$$(1-\phi) = \frac{N}{V} \times \frac{4\pi r^3}{3}, \quad (2)$$

where again ϕ is porosity. Since the average grain radius for the Ottawa F110 sand was $r = 60$ μm, the result of this computation is $n = N/V = 6.85 \times 10^{11}$ m^{-3}.

We use the number density *n* in order to estimate the specific surface area:

$$s = n \times 4\pi r^2 \simeq 3.1 \times 10^4 \, \mathrm{m}^{-1}. \quad (3)$$

Then, it follows that $(\phi/s)^2 \simeq 150 \times 10^{-12}$ m², which gives us one key factor needed in equation 1.

Finally, we backsolve equaiton 1 for the effective formation factor:

$$F = \frac{1}{2\kappa}(\phi/s)^2 \simeq 14.2. \quad (4)$$

This value *F* of the formation factor is needed in our subsequent calculations because its value reduces the effective permeability in all parts of sample porosity containing biopolymer. The result can be viewed as a type of tortuosity effect, i.e., the true path length followed by each fluid particle is greater than the straight line distance between the end points of the path. Formation factor has often been defined in terms of electrical measurements, but as we will argue next, its relationship to fluid permeability shown in equation 1, though neither as direct nor quite as universal, is nevertheless a very useful one for our present purposes.

Arguments that follow will begin with analogies to electrical properties of two-component composites. Because the physical nature of electrical conduction and fluid conduction are definitely not the same, this choice might at first seem somewhat inappropriate. However, because of the relative simplicity of the problems of interest to us here, we are nevertheless justified in putting these electrical analogies to use in this context. To see an earlier discussion of effective stress in porous media using similar arguments, consider the work in Berryman (1992). While the applications being focused on there were very different from the present ones, the physical justification of the methods used is nevertheless very analogous in the contexts of these two problems.

The ideas discussed next were originally introduced by Bergman (1978, 1980, 1982) and Milton (1980, 1981) and expanded upon by various researchers, including Korringa and LaTorraca (1986); Stroud, Milton, and De (1986); Johnson *et al*. (1986, 1987); and subsequently many others. The main point of the original approach was to develop a method to treat the complex (i.e., having both dissipative and inductive components of) conductivity (or, alternatively, complex dielectric constant) for heterogeneous systems having at least two distinct components, both of which have finite electrical conductivity and finite dielectric constant.

These two distinct physical effects tend to interact when both are present in the same physical system, and both necessarily will always be present whenever the system contains electrical conductors because all materials are dielectrics whether or not they are also conductors. It can therefore be important to perform the resulting mathematical analyses of these effects in the

complex impedance [i.e., (dielectric constant, angular frequency × conductivity) = (ε, $\omega\sigma$)] plane. The out-of-phase interactions between conductivity and dielectric constant typically will be strongly frequency dependent and, therefore, involve complex impedance analysis (i.e., including both the dissipative and inductive components simultaneously). How these effects interact for effective complex conductivity *G* was shown in detail [see Bergman (1980) and Milton (1980)] to follow a relatively simple but nevertheless completely general form (displayed here for the most commonly considered case having only two distinct constituents):

$$G(g_1, g_2) = \frac{g_1}{F_1} + \frac{g_2}{F_2} + \int_0^\infty dx \frac{\mathcal{D}(x)}{\frac{1}{g_1} + \frac{x}{g_2}}. \quad (5)$$

Constants g_1 and g_2 being considered can be, for example, real conductivities or real dielectric constants and also for complex impedances (i.e., including both conduction and induction, for example, in the form $g = \epsilon + i\omega\sigma$). Function $\mathcal{D}(x)$ is a real-valued density (or weighting) function. The complex versions of these physical constants also necessarily involve factors of angular frequency $\omega = 2\pi f$ via the magnetic induction terms. Note that, if either one of the constituents has the values $g_1 = 0$ or $g_2 = 0$ (i.e., one of these is actually a perfect insulator) associated with it, then the last term involving the integral in equation 5 vanishes identically, and thus, no knowledge of the density function $\mathcal{D}(x)$ itself is actually required. So we see immediately that $F_1$and F_2 are exactly the respective formation factors specific to each constituent, i.e., if $g_2 = 0$, then $G = g_1/F_1$, and by symmetry $G = g_2/F_2$ if instead $g_1 = 0$.

Another related comparison based on the same ideas was presented earlier by Berryman (2005) for applications to frequency-dependent thermal conductivity. In this alternative application, the same type of formula was used simultaneously for both thermal conduction and electrical conduction. However, in contrast, for the situations being considered in that case, a sand pack saturated with a conducting fluid could be analysed very effectively because, while undamaged sand grains tend to be relatively good thermal conductors, they are poor electrical conductors; meanwhile, pore fluids often have just the opposite behaviour, typically being good electrical conductors but poor thermal conductors. The main point to be made is that, not only is the form of the equations the same when moving from one physical situation (for example, electrical conduction) to the other (i.e., thermal conduction) but *the numerical values* of these formation factors F_1 and F_2 are also *the same pure numbers*; indeed they are simply geometrical constants, independent of the constituents' conductivity (thermal or electrical) values, or most other details of the particular physical context.

Now we will take advantage of the resulting analogy and note in particular that, once we have determined the pertinent purely geometrical formation factor *F* of the pore space shape for the granular system, this geometrical constant does not change its value when switching from one application to another one.

So F_1 and F_2 quantify the two types of *connectivities* in the problems under discussion. This approach gives us useful numbers to help quantify the expected behaviour of a porous sand pack that may have biopolymers (or colloids in other similar clogging applications) produced in the pore space during an attempt to reduce the fluid permeability via pore space reduction. So we can now take advantage of the mathematical structure as outlined here. This perspective differs from the more typical one and therefore provides some useful new insight since we can treat the sand grains themselves as perfect insulators (as far as both fluid conduction and permeability are concerned) in this different context. So if we take $g_1 = \kappa_1$ to be the effective constant for (obviously nonfeasible) fluid flow within any individual solid sand grain, then clearly $g_1 = \kappa_1 = 0$ since these grains, by definition, have no pores. Furthermore, the formation factor associated with the pore space itself is exactly the same one we have already determined by backsolving the first equation for $F = F_2$. Again, because fluid flow *within the solid grains* themselves is physically impossible, we must also have $g_1 = 0$. Thus the third term of the complicated formula 5 is eliminated, and we are left only with the especially simple result

$$\kappa = \frac{\kappa_2}{F_2}, \quad (6)$$

where κ_2 is the effective permeability of fluid flow through the porous assemblage of biopolymer (or colloid) material as it accumulates over time within the pores between the solid (nonporous) sand grains.

To determine the effects due to only the presence of biopolymer (or colloid), we need to multiply the *measured permeability* κ by the previously measured (or in our present examples sometimes actually computed) F_2, so that

$$\kappa_2 = F_2 \kappa = 3.27\,\mathrm{D}. \quad (7)$$

However, note that, since it is more likely that the pore-clogging effect has not been uniformly distributed within the pore space, this value should be viewed not as one uniform constant but as an overall average or effective value, i.e., not as a point-wise measure of the permeability that might then be associated with the pore-clogging material itself. This knowledge nevertheless gives us a direct means of determining the overall (i.e., the mean) influence of the biopolymer itself on the flow within the pore spaces among and between the sand grains. Beyond the impact of the biopolymer on flow, κ_2 is a bulk measurement of biofilm structure and suggests that measurements of permeability and/or resistivity could provide access to useful microstructural attributes of the microbial community.

Resulting overall retardation effects on the flow are stronger than those due only to this particular κ_2 value because the geometrical effects of the surrounding sand grains create additional

tortuosity effects that exist independent of the presence of the pore-clogging materials and therefore provide some significant progress towards the ultimately (as shown here) desired pore-plugging (and therefore our ultimate permeability-reducing) goal. These results give the significantly smaller values for the effective (reduced) permeability $\kappa = \kappa_2 / F_2$ to be observed directly in pore fluid flow studies.

It is important to make these distinctions as described, especially when performing external measurements such as seismic wave (in the field) or ultrasound (in the laboratory) attenuation measurements because such external measurements typically average these fluid permeability effects very differently. In fact, such measurements are known to sample the fluid effects on a local (rather than the more global) scale (Berryman 1986, 1988). *Average of the resulting overall effective permeability* is therefore found by computing the average of the inverse of permeability, which is therefore dominated by the lowest values of local permeability.

Logically, it is clear that, if permeability is zero locally anywhere along the fluid particle path, then it must follow that the global permeability necessarily vanishes along that path. So the pertinent physical quantity to average is necessarily the inverse of permeability rather than the permeability itself.

In contrast, wave attenuation averages permeability values directly, instead of inversely. Thus, we should definitely *not* expect perfect correlations between attenuation and permeability measurements in situations where the local permeability values are expected to fluctuate very strongly between these extremes of lower and higher values. However, if the fluctuations in local permeability are not so great, then we may expect the trends in permeability and attenuation to correlate better (though still only approximately).

It follows that the local κ_2 values are the ones important for seismic wave attenuation measurements rather than the overall global values of $\kappa = \kappa_2 / F$. An appreciation of this inherent complication then suggests one means of using the seismic wave attenuation values to reconstruct (to whatever extent this may be possible) the global permeability values (Berryman 1990), which normally are the ones that are being sought using such remote monitoring methods and wave attenuation data.

CORRELATIONS BETWEEN LOW-FREQUENCY (STATIC) PERMEABILITY (κ_0) AND WAVE

ATTENUATION QUALITY FACTOR (*Q*) AT HIGH FREQUENCIES

A brief review of some well-established pertinent acoustic attenuation methods will now be presented in this section. Johnson *et al*. (1987) show that the specific attenuation $1/Q$ at high frequencies (where the smaller scale pore structure becomes important to the wave propagation and attenuation) behaves according to a proportionality of the following type:

$$\frac{1}{Q} \propto \left[\frac{1}{\kappa_0^{1/2}} \left(\frac{2\eta}{\rho_f \omega} \right)^{1/2} \right]^{3-\delta}, \quad (8)$$

for a porous medium having complicated internal structure. (While their analysis is designed specifically for and phrased in terms of *fractal* surfaces, we shall nevertheless assume here, for the sake of argument, that this analysis also applies at least approximately to the complicated systems of interest with injecta clogging the pore space, whether the resulting conditions are strictly fractal or not.)

In 8, κ_0 is the low-frequency permeability, ω is again the angular frequency, η is the pore-fluid viscosity, and ρ_f is the fluid density. In this formula, the fractal dimension δ in the exponent is expected to lie in the range $2 < \delta < 3$, indicating behaviour characteristics somewhere between simple 2D (possibly rough) surfaces, and more complex 3-dimensional tortuous tubular pore structures. So approximately (i.e., on average, and in the absence of any more specific information for our particular application), we have $3 - \delta \simeq \frac{1}{2}$. Then, substituting into equation 8, this average value shows that $1/Q_p$ might be expected to fit a curve proportional to $\kappa^{-1/4}$. However, we have found (empirically, using the laboratory data beng presented) instead that the Q_p data do *not* actually fit this initial hypothesis very well.

Therefore, we need to try a different approach and so will now use this factor δ in the exponent instead as a data fitting (and/or optimization) parameter. When we do this, we find (see the bottom panel in Fig. 1) that some laboratory results for short times (i.e., the first one to two days) fit reasonably well for a power of 1/8, instead of the value 1/4 we had anticipated (from the previously presented arguments) might be operative. We can then infer that this choice implies that $3 - \delta = 1/4$ or that the apparent fractal dimensionality goes like $\delta = 2.75$ rather than the operative (best guess) value 2.50 (which was our original trial choice, based on taking a very simply determined average value).

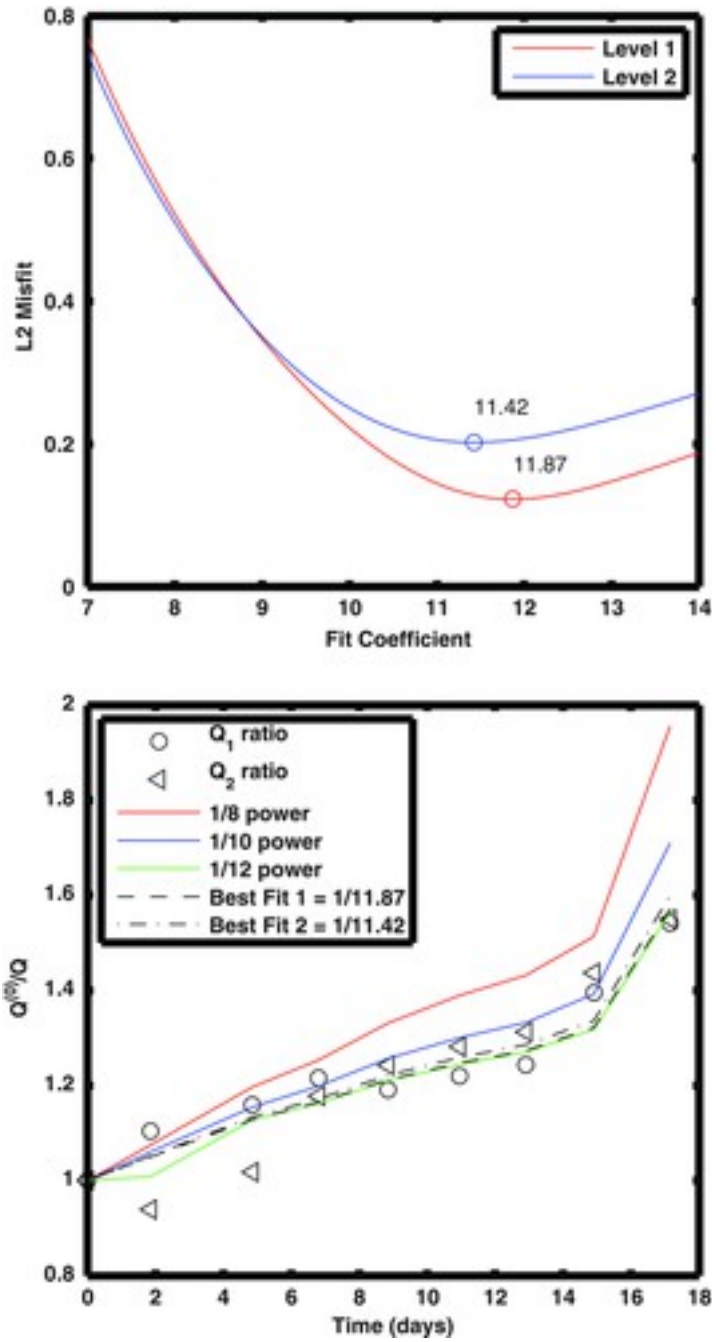

Figure 1

Open in figure viewerPowerPoint

Normalized ultrasonic wave attenuation inverse-*Q* at two granular column heights (of Ottawa sand) compared with normalized inverse of permeability κ to the 1/8th, 1/10th, and 1/12th powers and two best fitting powers. The misfit curves for determining the two best fitting values are shown in the upper panel. Data are from Kwon and Ajo-Franklin (2013).

Caption

If this were the final result for best correlations, then this should imply that $Q_p(0)/Q_p \simeq (\kappa(0)/\kappa)^{1/8}$ power. However, we find instead that, for two sets of measurements,

the results tend to converge over time, and the correlation factors change to something closer to rational powers of 1/10th or 1/12th, which do simultaneously fit both sets of the measured ultrasonic attenuation data trends reasonably well, i.e., within the caveats previously specified. However, the 1/8th power curve clearly diverges from the actual data for later times (e.g., those times greater than about six days into this first experiment).

We have chosen to limit consideration to such rational powers for the present discussion because the end result of our measurements and computations can then take a relatively simple form such as $\kappa/\kappa_0 \simeq [Q_p/Q_p(0)]^{12}$ when estimating final changes in permeability from measured changes in attenuation.

The quoted observations suggest that, in the absence of more precise information about the internal structure of these complex systems, one reasonable first approximation for the expected behaviour of the specific attenuation turns out to be the proportionality:

$$\frac{1}{Q_p} \propto \frac{1}{\kappa^{1/12}} \quad (9)$$

at high frequencies (by which we mean ultrasonic frequencies approaching 1 MHz). The lower panel in Fig. 1 shows that this type of behaviour is in fact being observed on average in these laboratory data. It is this empirical correlation that can be used to fix the pertinent power law relationship between Q_p and κ in equation 9. The practical significance of the result becomes clearer when it is used in reverse, measuring attenuation *Q* and then predicting the relative changes in permeability by taking the 12th (or perhaps a somewhat more precise number yet to be determined) power of the expression in equation 9.

Figure 1 also shows how these effective fractal dimensions δ for the laboratory system are evolving over the course of the experiment, as the biopolymer causes the pore surfaces to become rougher and rougher. We can also choose to do a least squares fit to these data, and the upper panel in Fig. 1 then shows that the optimum values (which differ somewhat for these two probe locations in the experimental column) are powers 1/11.42 and 1/11.87. One should note that Kwon and Ajo-Franklin (2013) performed a similar (though less detailed) analysis but normalized permeability and attenuation in a slightly different manner; their analysis of the same data generated an exponent closer to 1/8.8 when averaged over a larger series of experiments.

The final results over the course of this 17-day experiment have apparently evolved into a complex fractal-like surface having an equivalent fractal dimension thus determined to be $\delta = 3 - 2\epsilon \simeq 2.83$, which is actually a value very comparable to results found for fractal surface dimensions ($\delta \simeq 2.82$) of naturally occurring sedimentary materials by Radlinski *et al.* (1999) over scales of 1–10 microns using neutron scattering (USANS). Similar scattering

measurements using either neutrons or synchrotron X-rays (SAXS) may provide a different approach to confirm evolution of the effective fractal dimension during biopolymer deposition.

VARIATIONS OF ACOUSTIC ATTENUATION: ULTRASONIC AND HIGH-FREQUENCY SONIC MEASUREMENTS

In addition to the ultrasonic measurements of Kwon and Ajo-Franklin (2013) already discussed here, related frequency-dependent BE measurements were performed by Ta *et al*. (2014); Figs. 2–5 also show a similar increase in acoustic attenuation with decreasing bulk permeability as a result of the same pore-clogging effects of dextran (see Figs. 3c and 5c). By comparison, acoustic velocities do not show significant changes on the accumulation of dextran (see Figs. 2a and 4a). While the frequency range studied in Kwon and Ajo-Franklin (2013) is on the order of hundreds of kilohertz, the BE measurements of Ta *et al*. (2014) fall in a lower frequency range of a few tens of kilohertz for P-waves and a few kilohertz for S-waves. So BE measurements demonstrate variations of acoustic properties in the transitional frequency band between ultrasound and high-frequency sound.

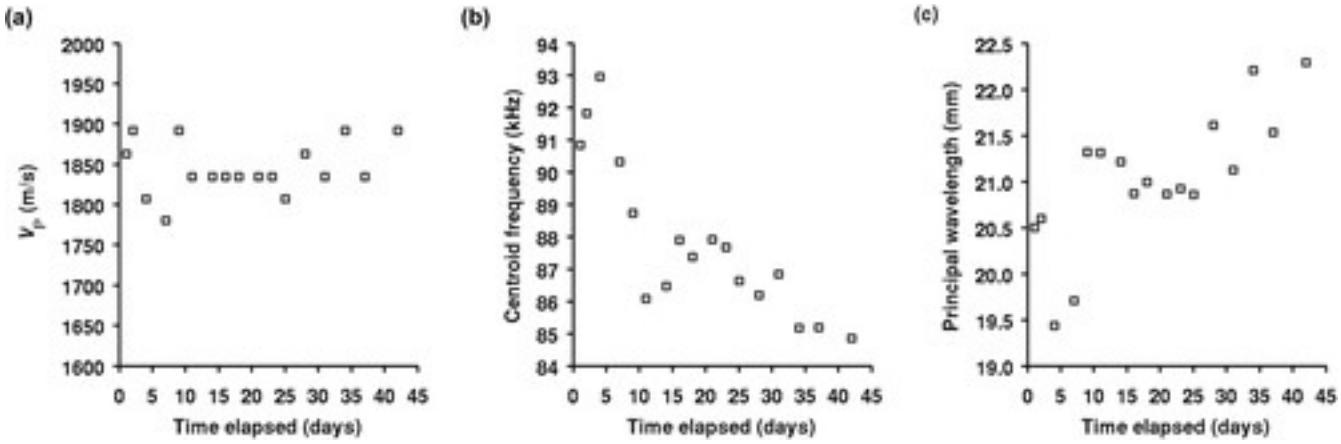

Figure 2
Open in figure viewerPowerPoint
Changes in *P*-wave (a) velocity, (b) centroid frequency, and (c) principal wavelength with time over the course of the Ottawa sand column experiment for the bender P-wave. Data are from Ta *et al*. (2014).
Caption

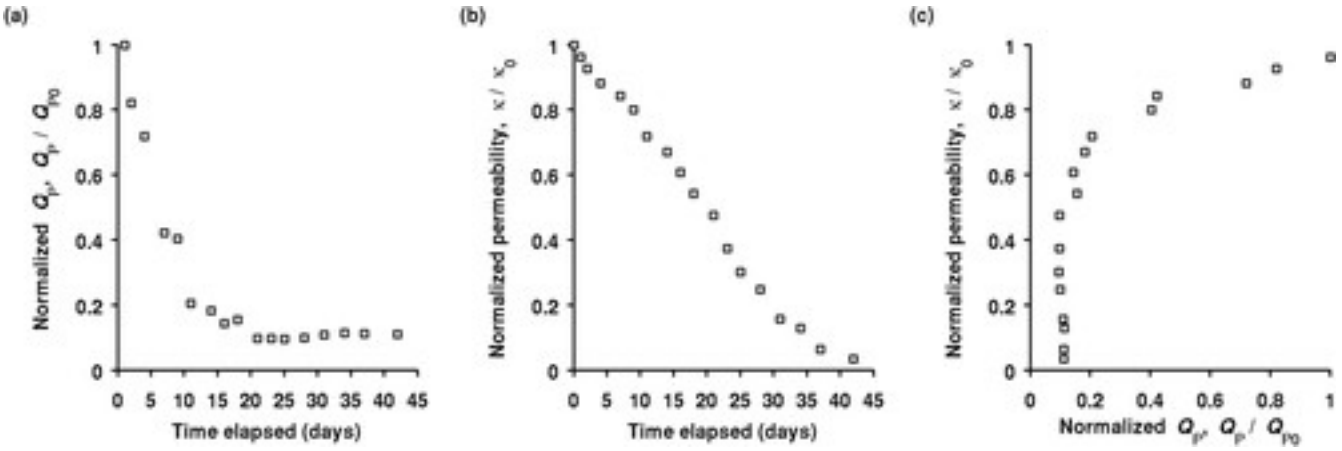

Figure 3

Open in figure viewerPowerPoint

(a) Normalized Q_p versus time, (b) normalized permeability versus time, and (c) normalized permeability versus normalized Q_p for bender P-wave 3. Normalization is done with respect to initial Q_p and permeability values (Q_{p0} and κ_0) obtained from day 1 of the Ottawa sand column experiment. These are based on data from Ta *et al*. (2014).

Caption

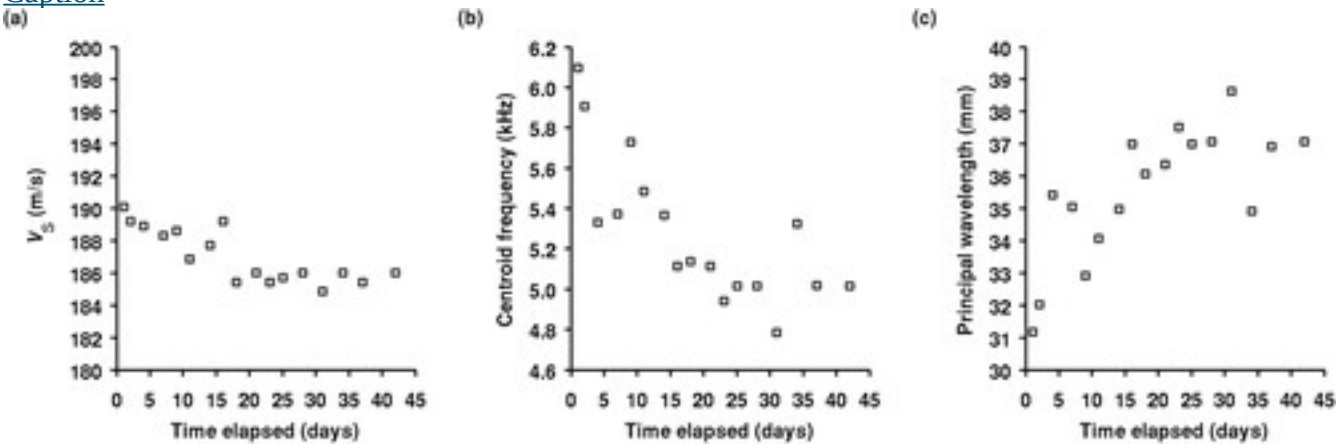

Figure 4

Open in figure viewerPowerPoint

Changes in *S*-wave (a) velocity, (b) centroid frequency, and (c) principal wavelength with time over the course of the experiment for bender S-wave 4. Data are from Ta *et al*. (2014).

Caption

By comparing observations from these two studies as described above, we can see that variations of acoustic attenuation are clearly frequency dependent. In ultrasonic measurements from Kwon and Ajo-Franklin (2013), the initial reduction of permeability in Figs. 3b and 5b yields a relatively small increase in acoustic attenuation in Figs. 3a and 5a. Subsequently, the increase in acoustic attenuation becomes more and more rapid for a given decrease in bulk permeability. In contrast, the BE measurements from Ta *et al*. (2014) show that the acoustic attenuation starts off increasing rapidly with decreasing permeability, and subsequently, the increase in attenuation

becomes much more gradual once the bulk permeability has been reduced to less than half of the initial value. In addition, the span of attenuation increase is also different between these two studies: over a similar span of permeability reduction, Q_p (for compressional wave attenuation measured via quality factor *Q*) shows aproximately a 35% reduction in the ultrasonic mesurements of Kwon and Ajo-Franklin (2013); in contrast, Q_p and Q_s (for shear wave attenuation measured via quality factor *Q*) exhibit about 90% reduction in the BE measurements of Ta *et al*. (2014).

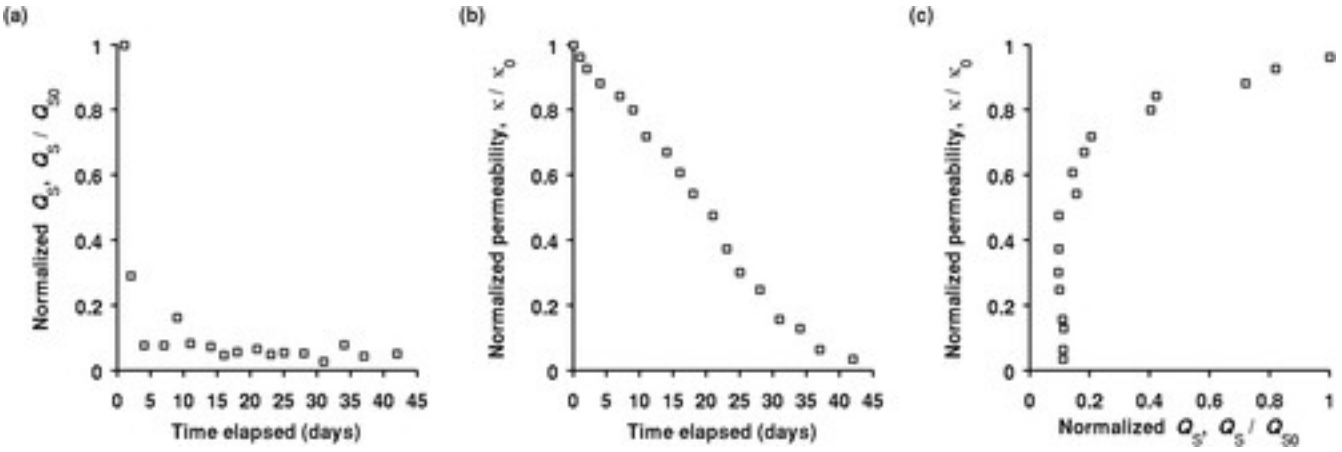

Figure 5
Open in figure viewerPowerPoint
(a) Normalized Q_s versus time, (b) normalized permeability versus time, and (c) normalized permeability versus Q_s. Normalization is done with respect to initial Q_s and permeability values (i.e., Q_{s0} and κ_0) obtained from day 1 of the Ottawa sand column experiment for bender S-wave 5. Data are from Ta *et al*. (2014).
Caption

NOTES ON POSSIBLE FIELD APPLICATIONS

While the main thrust of the present work concerns presentation of results for laboratory experiments, we should also point out some potential applications to field measurements. In particular, both Biot fast waves and Biot slow waves can be measured in the field (Nakagawa *et al*. 1997; Kelder and Smeulders 1997; Edelman 2003; Smeulders 2005; Bouzidi and Schmitt 2009). The present work has focused mainly on Biot fast waves measured in the laboratory. For such fast waves, the impact of the pore-clogging effects is to reduce the ability of the Biot fast waves to be attenuated via losses into induced pore fluid motion. In contrast, the Biot slow waves are very strongly affected by the same pore-clogging processes to the extent that such slow waves will ultimately be so greatly attenuated as to be impossible to measure. Therefore, fast waves are actually enhanced by pore-clogging effects because of such reduced attenuation, whereas any slow waves are highly attenuated and presumably ultimately prevented

from propagating altogether. Thus, observations of both types of waves simultaneously in the field (whenever feasible) should provide clear indications of the success (or not) of such pore-clogging efforts.

MAIN CONCLUSIONS

The goal of the work presented has been to analyse laboratory data on pore-clogging effects with an aim of determining whether or not there are useful correlations between the observed reductions in permeability and increases in the measurable wave attenuation that clearly must occur simultaneously. We have found that some such potentially useful correlations were indeed observed. The formation factor analysis presented here may be considered rigorous. The observed correlations between attenuation Q values and the permeability κ reductions due to pore clogging are empirical (i.e., not being precisely predictable), but they are also nevertheless largely consistent in a quantitatively testable way with the body of previously published work on surface fractals in porous materials and especially for data pertinent to sedimentary materials. Since these observed empirical correlations appear to be sufficiently similar to those of other results measured on rocks, they may therefore prove to be very useful in practice for estimating and, therefore, remotely monitoring temporal variations in biopolymer stimulation treatments. The progress of microbes in such biopolymer treatments designed specifically to induce enhanced pore clogging can therefore be measured in a reasonable and quantitatively useful way, which was one of the main purposes of this line of inquiry.

While not directly related to the main discussion above, it should nevertheless be mentioned that other workers' observations of the *Biot slow wave* in granular media (Nakagawa *et al*. 1997; Kelder and Smeulders 1997; Edelman 2003; Smeulders 2005; Bouzidi and Schmitt 2009). Also have potential to serve as a means of monitoring the progress of bio-enhanced pore-plugging efforts of the type that has been of most interest in our present studies, as we emphasized already in the preceding section.

Our work has concentrated on establishing reproducible correlations between ultrasonic attenuation changes due to pore clogging and concurrent changes in fluid permeability. To establish whether these results may also be pertinent to fluid-flow monitoring applications in the field nevertheless requires additional measurements (especially at lower frequencies) since these fluid-induced losses are known to show strong frequency dependence.

ACKNOWLEDGMENTS

Work is performed under the auspices of the U.S. Department of Energy (DOE) at the Lawrence Berkeley National Laboratory (LBNL), University of California, Berkeley. This material is based upon work funded by the Office of Biological and Environmental Research, Office of Science, U.S. DOE, under Contract DE-AC02-05CH1131. The authors would like to thank R. Chakraborty (LBNL) for assistance in culturing and microbial analysis and B. P. Bonner (LBNL) for suggestions during the data analysis phase. Primary support for the research was funded by the Energy Biosciences Institute. Some additional support was provided by the Geosciences Research Program of the DOE Office of Basic Energy Sciences, Division of Chemical Sciences, Geosciences, and Biosciences during the completion, review, and publication phases of the work. All support of this research is hereby gratefully acknowledged.

APPENDIX A: Λ PARAMETER

For many uses and especially for applications to well-logging data, it should prove helpful to point out some known connections between the analysis presented above, and the related analyses by Johnson *et al*. (1987) and also later by Pride and Berryman (2003a, b) and Pride, Berryman, and Harris (2004). We will skip over many of the details discussed in these papers in order to get to our main point, which is that we have another useful formula for permeability κ, closely related to equation 1, which is:

$$\kappa = \frac{\Lambda^2}{8F}, \quad (10)$$

[Compare the form of equation 1.] Parameter Λ (generally called the "Lambda parameter") is a weighted pore-volume-to-pore-surface ratio (Johnson *et al*., 1986). Like the formation factor, the precise definition of Λ is normally made with regard to electrical measurements (Johnson *et al*., 1987) and is typically stated as

$$\frac{2}{\Lambda} = \frac{\int dS_p |\nabla \psi(\mathbf{x})|^2}{\int dV_p |\nabla \psi(\mathbf{x})|^2}, \quad (11)$$

where $\psi(\mathbf{x})$ is the local electrical potential at spatial position **x**, and $\int dS_p$ is a surface integral over the pore boundary, whereas $\int dV_p$ is a volume integral over the pore volume. By equating equations 1 and 10, we find that Lambda parameter Λ plays exactly the same role in this formulation as does the ratio $2\phi/s$ in the formulation presented in equation 1. Thus, for applications in which Λ might be measured (or estimated) by well-logging means and when very little other information is known directly about either specific surface area *s* or porosity ϕ individually, such a measured value of Λ may be substituted as indicated to provide the needed estimate of the formation factor $F = \frac{\Lambda^2}{8\kappa}$. This result therefore gives us another means of determining some pertinent data for formation factor *F* in a typical field context.

Numerical tests of these same ideas related to the Λ parameter have been performed by Kostek, Schwartz, and Johnson (1992). Experimental tests relating the hydraulic and electrical properties of porous materials have also been performed (for example) in sand–clay mixtures by Wildenschild, Roberts, and Carlberg (2000). In general, these ideas have been repeatedly tested by various groups around the world and have also been applied to seismic attenuation data as we discuss more completely here in **Appendix B**.

The approach outlined in this presentation provides one possible alternative to performing actual fluid flow tests (being very difficult and expensive to perform in practice and especially so in the field) on the systems of most interest to us. Monitoring of electrical conduction properties of these systems (which is clearly feasible in either a laboratory or field setting) could thus provide some pertinent additional data to aid our understanding of what is happening inside the pore spaces of interest in such bioclogging contexts.

APPENDIX B: BIOT THEORY MODIFIED FOR HIGHER FREQUENCIES

Biot's original theory of wave propagation in fluid-saturated porous media (Biot (1956a, b) was designed to provide a relatively simple framework for understanding, modelling, and quantifying the seismic/acoustic behaviour of complex fluid-containing earth systems (or possibly other porous systems too, such as porous sound-proofing materials). Models chosen for study by Biot were rather simple ones, including pores in the shape of straight tubes or pores formed by the gaps between parallel plates. Biot's choices then allowed him to model these systems directly within the modelling context of the theory he was developing. Unfortunately, realistic porous systems seldom closely mimic such simple pore geometries. Nevertheless, the basic ideas of Biot can be carried over if certain rather simple analytical functions (very similar in behaviour to those developed by Biot) are used (Sheng and Zhou 1988; Charlaix, Kushnick, and Stokes 1988; Zhou and Sheng 1989; Johnson 1989). These results have been considered to be well understood now for over 20 years, so we will not elaborate extensively here.

Johnson (1989) writes the pertinent scaling function as:

$$f(\omega/\omega_c) = \frac{1}{[1 - iM\omega/2\omega_c]^{1/2} - i\omega/\omega_c}, \quad (12)$$

where ω is the angular frequency (i.e., $2\pi \times$ frequency), $\omega_c \equiv \eta\phi/\rho_f\kappa_0\alpha$ is a critical angular frequency, η is the viscosity of the pore fluid, ϕ is the porosity, ρ_f is the fluid density, κ_0 is the low-frequency (i.e., near dc) fluid permeability of the system, and α (a factor used in the definition of ω_c) is a measure of the tortuosity of the pore space. Parameter *M* is found

experimentally to be approximately equal to unity in many porous media. The previously quoted papers show that the *ansatz* 12 for the function $f(\cdot)$ is remarkably consistent with both theory and experiment. This fact is not so surprising however because this *ansatz* is *also*consistent with the two theoretical results obtained originally by Biot (1956b) for tubular pores, as well as for the pore space between parallel plates, which were themselves already two very extreme limiting cases of the possible geometries of interest.

APPENDIX C: SUM RULE FOR FORMATION FACTORS

It is not hard to show [also see Berryman (2005)] that the following sum rule for formation factors holds:

$$1 - \frac{1}{F_1} - \frac{1}{F_2} = \int_0^\infty \frac{dx\mathcal{D}(x)}{1+x} \geq 0. \quad (13)$$

This result follows directly from equation 5 when $g_1 = g_2 = 1$ and shows an important quatitative relationship between the distinct formation factors F_1 and F_2 and the real-valued density function $\mathcal{D}(x)$ that arises in the theories of Bergman (1978, 1980, 1982) and Milton (1980, 1981). Both equations 5 and 13 presume that the system has only two distinct porous constituents. If more than two constituents were actually present, then we would need to generalize both equations accordingly in order to incorporate these additional degrees of freedom in the systems into these equations. Such extensions, however, are beyond our current scope.